cle-tyke Motion Estimation by the Fusion of Image Point and Line Features. *Pattern Recognition*, 31(3), p.p.333-344.
7. Huang Wenzhong, Miao Guoxing (2005) Establishment and Application of Information Management System in Jianxin Colliery. *Jiangxi Coal Science & Technology*, No.3, p.p.52-54.
8. Zhang Li (2010) Application of Information Fusion Technology in Pingdingshan No.5 Coal Mine. *Zhongzhou Coal*, 177(9), p.p.71-73.
9. Yan Xin, Fu Hua, Kan Yi (2012) Prediction of Coal and Gas Outburst Based on Multi-agent Information Fusion. *Control Engineering of China*, 19(3), p.p.431-434.
10. Zadeh L A (1984) Review of books: A mathematical theory of evidence. *AI Magazine*, 5(3) , p.p.81-83.
11. Yager R R (1987) On the D-S framework and new combination rules. *Information Sciences*, 41(2), p.p.93-138.
12. Lefevre E, Colot O, Vannoorenberghe P. (2002) Belief functions combination and conflict management. *Information Fusion*, 3(2), p.p.149-162.
13. Zhang S D, Wang L D (1997) Absurdities about Dempter-Shafer's rule of combination of evidence. *Systems Engineering-Theory & Practice*, 17(5), p.p.82-85.
14. Li W Y, Guo K H (2010) Combination rules of D-S evidence theory and conflict problem. *Systems Engineering-Theory & Practice*, 30(8), p.p.1422-1432.
15. Liang C Y, Chen Z M, Huang Y Q, et al. (2005) A method of dispelling the absurdities of Dempster-Shafer's rule of combination. *Systems Engineering-Theory & Practice*, 25(3), p.p.7-12.
16. Ren Kai-Jun, Wu Meng-Da, Liu Qi (2002) The combination of prior distributions based on Kullback information. *Journal of the Academy of Equipment Command & Technology*, 13(4), p.p.90-92.
17. Li Yang, Guo Ya-Jun, Yang You-Liang (2014) Identification and application of the evidence conflict based on K-L information distance. *Systems Engineering-Theory & Practice*, 34(8) , p.p.103-107.
18. He Qi-Lin, Wang De-Ming (2004) Numerical Simulation of Spontaneous Combustion Process in Goaf Areas by Fully-Mechanized and Caving Roof Coal. *Journal of China University of Mining & Technology*, 33(1), p.p.11-14.

A Direct Method for Estimating Net Radiation from HJ-1B Cloud-Free Data

Ziyu Huang, Kexue Liu, Yueming Hu, Jianbo Xu

The College of Natural Resources and Environment of South China Agricultural University, Guangzhou 510642, Guangdong, China

Abstract
A simple scheme is proposed to estimate instantaneous net radiation over the Heihe River watershed under clear sky conditions using HJ-1B data. We developed an algorithm that primarily use remote sensing information and eliminates the dependency on measured data from ground

stations as model input. Surface albedo is one of the key variables for the estimation of upward shortwave radiation. The MODIS BRDF/albedo product MCD43A1 severed as priori knowledge to address the problem that HJ-1B satellite only has a single viewing angle, by using kernel-driven BRDF model and 6S radiation transfer code. The accuracy of this approach was evaluated using ground measurements. The improved generalized single-channel algorithm was adopted to retrieve land surface temperature. Then, the temperature–vegetation index (TVX) for the area-wide mapping of instantaneous air temperature was adopted. The approach was complemented by an iterative filtering routine for eliminating outliers, and by an interpolation algorithm for filling data gaps. The air temperature retrieval was also validated using the measured air temperatures. Since instantaneous net radiation estimates have limited scope compared to daily average values or diurnal cycle, a sinusoidal model is proposed to estimate the diurnal cycle of net radiation. The sinusoidal model is capable of retrieving the diurnal variations of net radiation with a single instantaneous net radiation estimate from satellite data. The methodology presented here can be used to estimate net radiation with accuracy comparable to that of available methods.
Key words: REMOTE SENSING, HJ-1B, NET RADIATION.

1. Introduction

Surface net radiation refers to the net energy that the Earth surface gains from shortwave and longwave radiations. Being an important component of the surface radiation budget and a primary energy source that drives atmospheric movement, the net radiation spatial distribution and its variation with time are significant factors to consider when studying weather and climate systems [1]. Meanwhile, net radiation controls the sensible heat and latent heat fluxes that enter the atmosphere, thus many models that estimates surface evapotranspiration from remote sensing data need to estimate net radiation first [2]. Undoubtedly, net radiation monitoring stations provide the most accurate measurements of surface net radiation flux. However, the number of such stations is limited and their maintenance is costly. Those stations cannot fulfill the demands from climate research, weather forecast, and other related areas. A more practical way is to estimate the surface net radiation, and it is widely being studied.

Satellite remote sensing is the most suitable means for studying regional surface net radiation flux. At present, various products that estimate surface radiation budget from satellite data have emerged, such as GEWEX-SRB[3], ISCCP-FD[4], and CERES-FSW[5]. Although widely accepted in practical use, such products generally have low resolution and low precision, thus failing to satisfy the requirements of large-scale climate researches, especially remote sensing evapotranspiration studies. Besides these mature and publicly available products, many studies are using data from various remote sensing platforms to estimate surface radiation budget [6-10]. Although such studies employ different approaches and work in different modes, some still being immature, it is obvious that satellite remote sensing has become an important method for studying surface radiation balance.

Generally, the surface net radiation estimation methods that utilize remote sensing data need to combine the data with ground measurements. This posts a huge limitation on the application of those methods to large-scale surface radiation retrieval. On the one hand, the regions with fewer weather stations lack of regular measurements. On the other hand, ground measurements and remote sensing data are often in different temporal and spatial scales; interpolation of ground measurements to larger scales would produce overly smooth data that does not describe the spatial unevenness. A possible solution to this problem is to estimate surface net radiation solely using satellite remote sensing data, excluding ground measurement. In Sep 2008, China launched the environment and disaster monitoring and forecasting small satellite constellation A and B, known as HJ-1A and HJ-1B satellites. The satellite spatial resolution is 300 ^{m}, with a swath width of 720 ^{km} and a repetition cycle of 4 days. Comparing with the MODIS data with shorter repetition cycle, and the TM and ASTER data with higher spatial resolutions, HJ-1B data has a more optimized temporal and spatial resolution combination and provides data support for high-spatial resolution surface energy balance studies. This paper presents an algorithm scheme suitable to the surface net radiation estimation using HJ satellite data. We hope to provide reference for the estimation of regional evapotranspiration from remote sensing data, so as to broaden the application of HJ satellite data.

2. Methodology

2.1. Instantaneous Surface Net Radiation

As an important indicator of the earth-atmosphere system radiation budget, surface net radiation is the difference between the various radiations that

the Earth surface receives from the sun and the atmosphere and the various radiations it radiates and reflects. Generally, surface net radiation can be expressed as

$$R_n = R_S^{\downarrow} - R_S^{\uparrow} + R_L^{\downarrow} - R_L^{\uparrow} = (1-\alpha)R_S^{\downarrow} + \sigma\varepsilon_s\varepsilon_a T_a^4 - \sigma\varepsilon_s T_s^4 \quad (1)$$

Where

$R_S^{\downarrow}$ -- Downward shortwave radiation;

$R_S^{\uparrow}$ -- Upward shortwave radiation;

$R_L^{\downarrow}$ -- Downward long-wave radiation;

$R_L^{\uparrow}$ -- Upward long-wave radiation;

α -- Surface albedo, calculated by introducing MODIS BRDF as priori knowledge to complement the lack of angle information when retrieving albedo using HJ satellite data [11];

ε_s -- Surface emissivity, estimated using the NDVI threshold method [12];

T_a -- Surface temperature (K), retrieved using the improved generalized single-channel algorithm based on the characteristics of HJ-1B satellite thermal infrared waveband [13];

σ -- The Stefan-Boltzman constant ($5.67 \times 10^{-8} W \cdot m^{-2} \cdot K^{-4}$);

T_s -- Atmosphere temperature (K), retrieved by using the temperature-vegetation index (TVX) method [14];

ε_a -- Atmospheric emissivity, calculated with the following equation proposed by Idso [15]:

$$\varepsilon_a = 1 - 0.26\exp\left[-7.77 \times 10^{-4}(273 - T_a)^2\right] \quad (2)$$

The downward shortwave radiation $R_S^{\downarrow}$ is calculated with the following equations [16]:

$$R_S^{\downarrow} = G_{sc}\cos(\theta) d_r \tau_{sw} \quad (3)$$

$$d_r = 1 + 0.033\cos\left(\frac{2\pi}{365}J\right) \quad (4)$$

$$\tau_{sw} = 0.75 + 2 \times 10^{-5}(Z) \quad (5)$$

Where G_{sc} is the solar constant at the top of the atmosphere ($1367 W \cdot m^{-2}$), θ is the solar zenith angle (rad), J is the number of days of the year, and Z denotes the elevation (m).

2.2. Daytime average net radiation

Instead of instantaneous surface net radiation, more models and applications prefer daytime average net radiation. In particular, many studies that use satellite remote sensing data to estimate evapotranspiration requires input of daytime average net radiation. Interpolating instantaneous surface net radiation data is the most intuitive way to estimate total daytime net radiation. However, simple linear interpolation does not well represent the daily variation of surface net radiation. Studies have shown that from sunrise to sunset, the variation of surface net radiation exhibits roughly as a curve similar to a sinusoidal function. Therefore, given a point on the curve, i.e. the net radiation flux at any time point, the entire curve can be derived, thereby obtaining the total daytime net radiation.

According to the above assumption, with the instantaneous net radiation INR at the time the satellite passes by ($t_{overpass}$), the instantaneous net radiation $R_n(t)$ at any time t can be obtained by using the following equation:

$$R_n(t) = INR\frac{\sin\frac{(t-t_{sunrise})\pi}{t_{sunset}-t_{sunrise}}}{\sin\frac{(t_{overpass}-t_{sunrise})\pi}{t_{sunset}-t_{sunrise}}} \quad (6)$$

Where $t_{sunrise}$ is the local time of sunrise (hrs) and t_{sunset} is the local time of sunset (hrs), both can be calculated based on the geographic location and date.

Since the total daytime surface net radiation is the sum of all the instantaneous net radiation fluxes during day time, when the distribution function of instantaneous net radiation is determined, the total daytime net radiation can be calculated by

$$DailyR_n = \int_{t_{sunrise}}^{t_{sunset}} R_n(t)dt \quad (7)$$

Whereas the daytime average net radiation is estimated by

$$DANR = \frac{\int_{t_{sunrise}}^{t_{sunset}} R_n(t)dt}{\int_{t_{sunrise}}^{t_{sunset}} dt} = \frac{2INR}{\pi\sin\frac{(t_{overpass}-t_{sunrise})\pi}{t_{sunset}-t_{sunrise}}} \quad (8)$$

3. Study Area and Data

The ground measurements were from the eco-hydrology remote-sensing experiments carried out for Heihe River [17]. Table 1 presents the information of the ground stations, including longitude and latitude, elevation and underlying surface type. The measured data include the four components of radiation, including upward/downward shortwave/long-wave radiation, land surface temperature, and air temperature. The frequency of ground measurements (per 10 minutes) does not match the imaging time of the HJ satellite, thus the values measured at the two time points before and after the HJ satellite imaging time were used to perform linear interpolation. The interpolation result was used as the measured values at the station.

Table 1. Ground stations information

Station name	Longitude and latitude	Elevation/*m*	Land cover type
Daman Super Station	100.37223°E, 38.85551°N	1556.06	Corn
Gobi Station	100.3042°E, 38.91496°N	1562	Gobi Desert
Shenshawo Desert Station	100.4933°E, 38.78917°N	1594	Desert

Nine grids of HJ-1B data of the study area, taken in 2012 on cloud-free days, were obtained from the website of the China Centre for Resources Satellite Data and Application (CCRSDA). The MOD021KM, MOD03 and MOD04 data products of the same date and the MCD43A1 product that contains data of the same date were also obtained. The MODIS data was downloaded from the website of the USGS Land Processes Distributed Active Archive Center (https://lpdaac.usgs.gov/). The MOD021KM data was used to compute atmospheric water vapor content. The MOD03 is the level-1 product for geographic locating; it provides geographic information of every 1 *km*, including latitude, longitude, solar zenith and azimuth angles, and zenith and azimuth angles of the satellite. The MOD04 data is an MODIS aerosol optical depth product. This product was used for the atmospheric correction of HJ satellite data and the calculation of the proportion of sky scattered light needed by albedo retrieval. The MCD43A1 data is a BRDF product, with a time interval of 8 days and a resolution of 500 *m*. Each data of this product depends on the valid data measured by the MODIS sensors on Terra and Aqua satellites in the followed 16 days. BRDF parameters are provided by this product and were used for the surface albedo retrieval.

Table 2. Remote sensing data (partial) used in this study

Data	HJ-1B	Path/Row	MCD43A1
2012/06/19	HJ-1B CCD2	22/67	2012/06/17~2012/07/02
	HJ-1B IRS	20/69	
2012/06/30	HJ-1B CCD2	20/68	2012/06/25~2012/07/10
	HJ-1B IRS	18/70	
2012/08/03	HJ-1B CCD2	22/68	2012/07/19~2012/08/03
	HJ-1B IRS	19/70	
2012/08/15	HJ-1B CCD1	23/68	2012/08/12~2012/08/27
	HJ-1B IRS	25/70	
2012/09/02	HJ-1B CCD2	21/68	2012/08/28~2012/09/12
	HJ-1B IRS	19/67	
2012/09/06	HJ-1B CCD1	18/68	2012/09/05~2012/09/20
	HJ-1B IRS	21/70	
2012/09/14	HJ-1B CCD1	22/68	2012/09/13~2012/09/28
	HJ-1B IRS	25/69	
2012/09/17	HJ-1B CCD2	21/68	2012/09/13~2012/09/28
	HJ-1B IRS	19/70	
2012/09/21	HJ-1B CCD2	23/68	2012/09/21~2012/10/06
	HJ-1B IRS	21/70	

First of all, the HJ-1B data was calibrated based on the geometrically calibrated Landsat TM data. Using TM image as standard image, image-to-image geometric calibration was performed. The nearest neighbor method was employed to re-sample data with the original gray scale of pixels kept. After calibration, the root mean square error ($RMSE$) was smaller than 1 pixel. The Landsat TM data was obtained from the website of USGS (http://glovis.usgs.gov/). Since MODIS data contains detailed longitude and latitude waveband information, the MODIS Conversion Toolkit (MCTK) of ENVI was used to perform automatic geometric calibration of MODIS data. The MODIS images were matched with Landsat TM images, the latter being the standard images. The zenith angle [18] corresponding to each satellite pixel was derived from the passing by time of HJ-1B satellite and geographic information of the pixel. Based

on the satellite angle data provided by the CCRSDA, inverse distance weighted (IDW) interpolation was performed to calculate the view angle of the HJ-1B satellite. The on-orbit absolute radiometric calibration coefficients of HJ-1A and B, published by the CCRSDA in 2012, were used for radiometric calibration. DN images were converted to radiance format and then atmospheric correction was performed using 6S model. Considering the relatively small size of the study area, plus that the chosen data had high atmospheric visibility and small aerosol optical depth, the mean values of the MODIS product (MOD04) of the study area was used as the aerosol optical depth. The comparison between the spectra and NDVI values of different types of objects before and after atmospheric correction showed that the influence of atmosphere was successfully eliminated.

4. Results and Analysis

4.1. Surface albedo

Surface albedo is a key parameter for the estimation of upward shortwave radiation. When using remote-sensing data of single angle to retrieve surface albedo, the land surface is often assumed as an isotropic Lambertian surface. Such method uses remote-sensing data with approximately the zenith angle to estimate the reflectance of land surface, which is then used to represent the hemisphere albedo of the Earth surface. Kimes [19] pointed out that such assumption might result in errors as high as 45%. Studies [20] have shown that for single-angle remote-sensing data, priori knowledge of anisotropic land surface can be introduced to improve the surface albedo retrieval accuracy. In this study, the albedos of each individual waveband [11] of HJ satellite were obtained by using nuclear-driven model, BRDF parameters provided by MCD43A1, and the sensor and solar angle information of the satellite. Then, the 6S model was employed to perform radiation simulation. The ratio of each waveband incident energy to the total incident energy was used as the weight of the waveband to retrieve wide-band surface albedo [21]. For each weather station, the average value of the peripheral 3×3 window of the corresponding pixel was used as the retrieved value. Figure 1 compares the retrieved albedos with the measured values. It can be seen that the retrieved albedos for the Daman Super Station are the most accurate, overall slightly higher than measured values. For Daman Super Station, the MAE is 0.0047 and $RMSE$ is 0.0052. The retrieved albedos for the Gobi Station are slightly lower than the measured values, with MAE of 0.0049 and $RMSE$ of 0.0054. The accuracy of the retrieved albedos for the Shenshawo Desert Station is the lowest. The retrieved values for this station are generally higher than the measured values, with the MAE of 0.0065 and $RMSE$ of 0.0084.

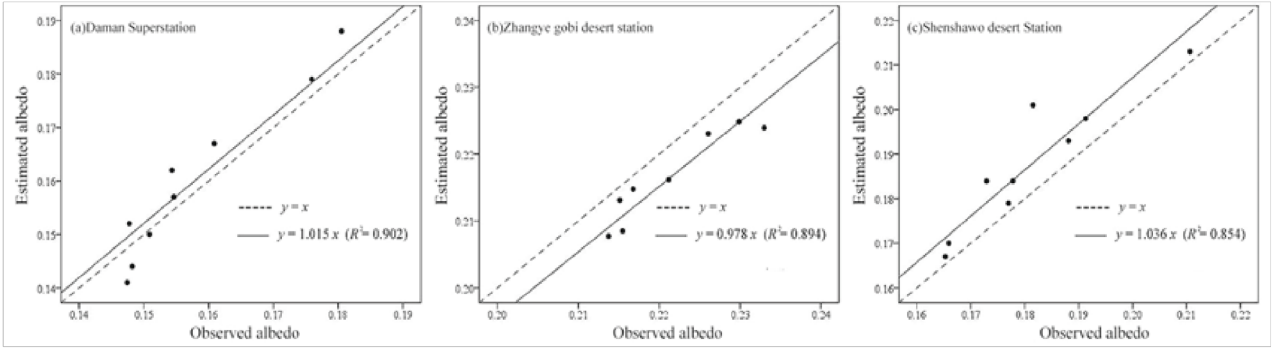

Figure 1. Comparisons between retrieved albedos from HJ satellite data and ground measurements

4.2. Surface temperature

Surface temperature is a key parameter for the estimation of upward long-wave radiation. In previous studies of land surface temperature (LST) retrieval using single thermal infrared channel, Landsat TM data have been used commonly. Such retrieval methods include radiative transfer equation, mono-window algorithm, and generalized single-channel algorithm. The radiative transfer equation is relatively complicated and requires many parameters, thus is not very applicable to LST retrieval. The generalized single-channel algorithm is more simplified than the mono-window algorithm; it requires only one atmospheric parameter, thus its application is very simple. The spectral range of the thermal infrared waveband of HJ-1B satellite ($10.5 \sim 12.5\ \mu m$) is very close to that of the Landsat TM satellite ($10.4 \sim 12.5\ \mu m$). In addition, both of them have only one thermal infrared waveband. Therefore, many researchers applied the LST retrieval algorithms for TM data to the LST retrieval using HJ-1B data. Although the single-channel algorithm works by the same mechanism for different sensors, some of the empirical formulae of the algorithm must be re-fitted according to the characteristics of the sensors corresponding thermal infrared wavebands. Zhou [13] proposed an improved gener-

alized single-channel algorithm based on the thermal infrared waveband of HJ-1B satellite. This improved algorithm was applied in this study for LST retrieval of the study area. Figure 2 presents the comparisons between retrieved LST and measured LST. It can be seen that the retrieval accuracy for the Gobi Station is the highest. For this station, the retrieved values are in general slightly lower than the measured values, with MAE of $1.47\ K$ and $RMSE$ of $1.55\ K$. The retrieved values for the Daman Super Station are slightly higher than the measured values, with MAE of $1.74\ K$ and $RMSE$ of $2.11\ K$.The accuracy of retrieved LST for the Shenshawo Desert Station is the lowest. The retrieved values for this station are lower than the measured values, with MAE of $2.22\ K$ and $RMSE$ of $2.54\ K$.

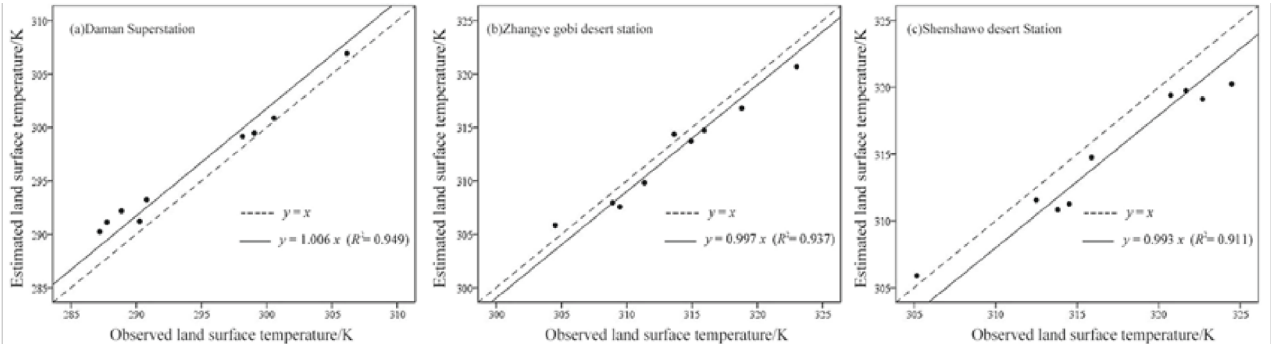

Figure 2. Comparisons between retrieved LST from HJ satellite data and ground measurements

4.3. Near-surface air temperature

Near-surface air temperature is a key parameter for the estimation of upward/downward long-wave radiation. There are two key factors in using TVX method to estimate near-surface air temperature, one is the size of the neighborhood, and the other is the saturated NDVI value corresponding to the pixels of thick canopy. Based on previous studies, a 13×13 pixels window was chosen for the neighborhood operation [14]. The parameterization method proposed by Nieto [12] was employed to compute the saturated NDVI of the study area. The retrieved temperature was evaluated using ground measurements. As seen in Figure 3, the retrieved temperatures for all three stations are higher than measured values, which is a common problem for TVX method. The study of Wloczyk [23], by comparing the air temperatures measured at the height of $5\ \mathrm{cm}$ and $2\ \mathrm{m}$ with temperature retrieved from remote sensing data, reckoned that this is due to the incapability of the retrieved temperature to acurately reflect the temperature at a specific height. The retrieval accuracy for the Daman Super Station is the highest, with MAE of $1.74\ K$ and $RMSE$ of $1.99\ K$. For the Gobi Station, the two values are $2.50\ K$ and $2.76\ K$. The retrieval accuracy for the Shenshawo Desert Station is the lowest, with MAE of $3.14\ K$ and $RMSE$ of $3.49\ K$

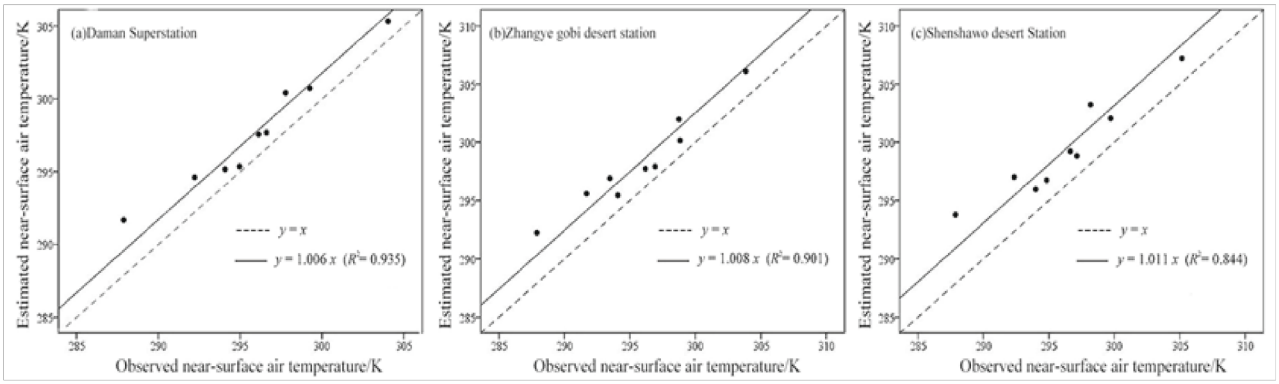

Figure 3. Comparisons between retrieved near-surface air temperature from HJ satellite data and ground measurements

4.4. Surface net radiation

The retrieved four components of radiation were evaluated using ground measurements. Over-estimation was found to the downward shortwave radiation retrieval for all three stations. This problem has also been found in many other studies. The study of Ryu[24] using MODIS data produced $RMSE$ of $19\sim65\ W \cdot m^{-2}$, which was also the $RMSE$ range of our study. Since upward shortwave radiation is obtained by multiplying downward shortwave radi-

ation with surface albedo, the same problem exists for upward shortwave radiation retrieval. Notably, the surface albedos retrieved for the Gobi Station is lower than the measured values, thus the upward shortwave radiation estimated for the station is more accurate comparing with those of the other stations. Meanwhile, because of the over-estimation of the near-surface air temperature, similar problem also exists for the downward long-wave radiation retrieval. The upward long-wave radiation, influenced by both land surface temperature and near-surface air temperature, is also over-estimated. Since the estimations for both LST and near-surface air temperature are overly high for the Daman Super Station, the retrieval accuracy for the station is the least accurate.

Table 3. Errors of energy balance ($W \cdot m^{-2}$)

Variables	Daman Super Station		Gobi Station		Shenshawo Desert Station	
	MAE	*RMSE*	*MAE*	*RMSE*	*MAE*	*RMSE*
Downward shortwave radiation	32.92	36.32	39.4	42.03	43.9	46.86
Upward shortwave radiation	7.84	8.98	5.23	5.98	13.65	15.25
Downward long-wave radiation	11.49	12.91	16.27	17.82	18.86	20.23
Upward long-wave radiation	17.72	19.83	12.05	15.36	15.05	18.46

As seen in Figure 4, over-estimation occurred to the instantaneous surface net radiation retrieval from HJ satellite data. Statistical analysis showed that the retrieval accuracy for the Daman Super Station is the highest. with MAE of $30.46\ W \cdot m^{-2}$ and $RMSE$ of $34.89\ W \cdot m^{-2}$. The two values for the Gobi Station are $37.34\ W \cdot m^{-2}$ and $40.73\ W \cdot m^{-2}$. The retrieval accuracy for the Shenshawo Desert Station is the lowest with MAE of $39.64\ W \cdot m^{-2}$ and $RMSE$ of $44.01\ W \cdot m^{-2}$, which are close to the results of previous studies[7, 10, 24].

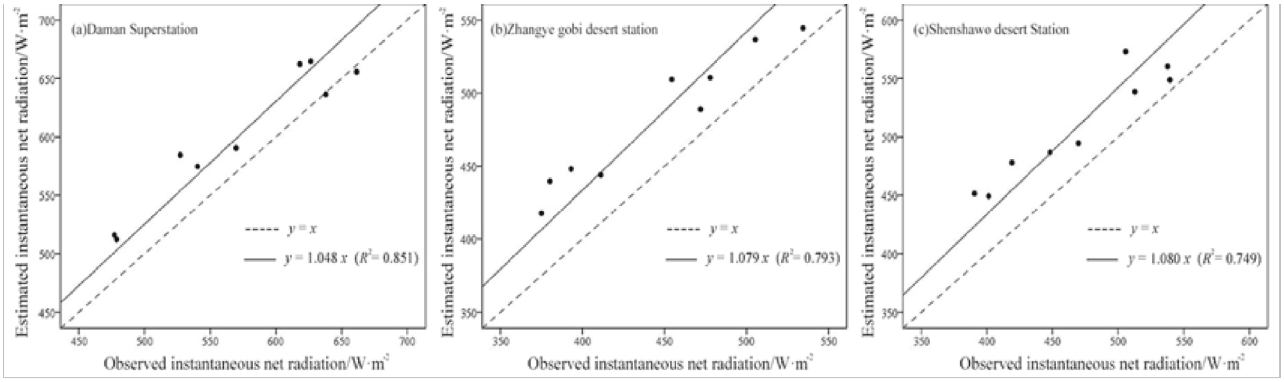

Figure 4. Comparisons between retrieved instantaneous net radiation from HJ satellite data and ground measurements

Since surface net radiation starts to increase only a while after sunrise, and becomes zero a while before sunset, removing a certain time period of data after sunrise and before sunset during the calculation of total daytime net radiation could help improve the estimation accuracy. In this study, the sunrise and sunset times were calculated using longitude and latitude of the station, as well as the date information [25]. Then 50 minutes after sunrise and 65 minutes before sunset were neglected for the calculation.

The data of a random date was chosen to validate the sinusoidal model. The dots in Figure 5 represent the measured values and the curve represents the instantaneous net radiation estimated using HJ satellite data. Apparently, the sinusoidal model fits the actual data almost perfectly. With accurate estimation of instantaneous net radiation, the daytime variation of net radiation can be derived accurately using the sinusoidal model. Therefore, estimating total daytime net radiation using this method is a feasible approach.

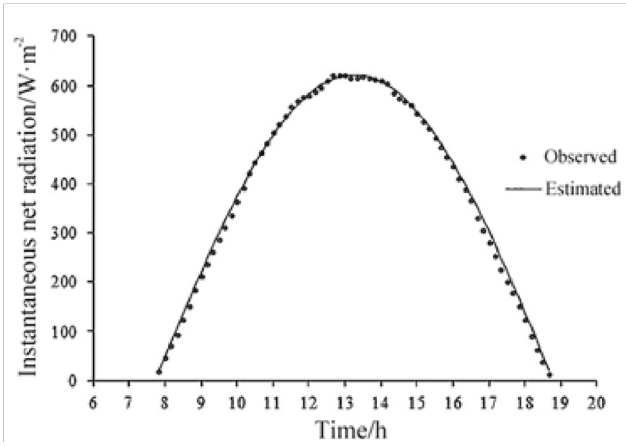

Figure 5. Diurnal cycle of net radiation

Figure 6 presents scatter plots of average daytime net radiation comparing with measured data. It can be seen that because of the over-estimation in instantaneous net radiation retrieval, the average daytime net radiation is also over-estimated. Statistical analysis showed that the retrieval accuracy for Daman Super Station is the highest, with MAE of $29.26\ W \cdot m^{-2}$ and $RMSE$ of $32.51\ W \cdot m^{-2}$. The two values for Gobi Station are $35.46\ W \cdot m^{-2}$ and $36.48\ W \cdot m^{-2}$, respectively. The retrieval accuracy for Shenshawo Desert Station is the lowest, with MAE of $37.66\ W \cdot m^{-2}$ and $RMSE$ of $39.36\ W \cdot m^{-2}$. Since the average daytime net radiation is an average of instantaneous net radiations, the errors are lower than that of instantaneous net radiation retrieval.

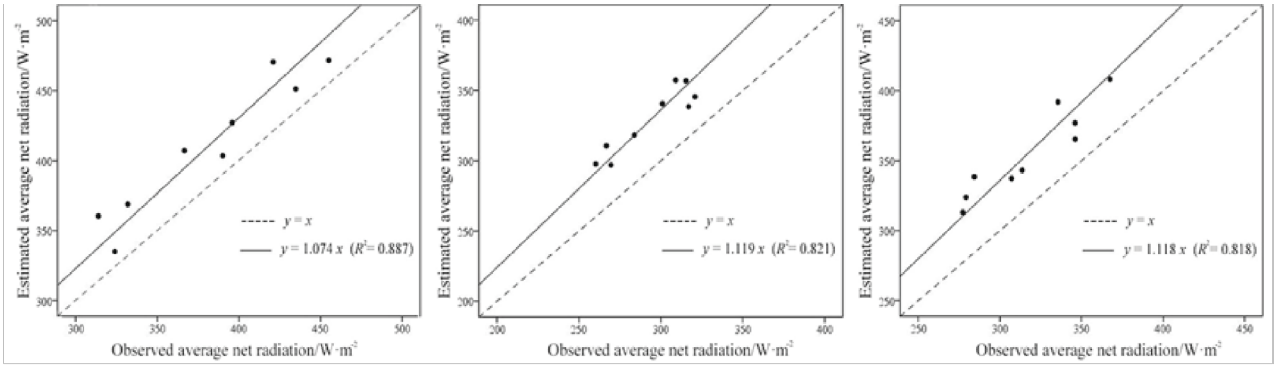

Figure 6. Comparisons between retrieved average daytime net radiation from HJ satellite data and ground measurements

The above analysis demonstrated that the proposed approach could efficiently calculate surface net radiation flux. This approach does not rely on ground measurements and the retrieval result is to a certain extent accurate. Therefore, it is helpful in better understanding the spatial variability of radiation flux.

5. Conclusions

Many algorithms that estimate surface net radiation and its components using various remote sensing data are available, with their own advantages and disadvantages. Based on existing theories and algorithms, and considering specific conditions and requirements of our study, we proposed in this paper an approach that estimates surface net radiation flux from HJ satellite data under clear sky conditions. Nine grids of HJ-1B data of the Heihe River watershed taken in 2012 were used to retrieve surface albedo, surface temperature, and near-surface air temperature. Based on the retrieved data, parameterization method was applied to estimate the downward/upward shortwave/long-wave radiations. Instantaneous net radiation was calculated. The retrieval accuracy was evaluated using ground measurements and over-estimation was found in the retrieval results. Comparing with measured values, the MAE of the retrieved instantaneous net radiation is $35.82W \cdot m^{-2}$, and the $RMSE$ is $39.88\ W \cdot m^{-2}$. Such result is close to those of previous studies. We hope that the results help to better understand the spatial variability of radiation flux.

In this study, interpolation using sinusoidal model was adopted to estimate the total daytime total net radiation based instantaneous net radiation flux. The net radiation of a random day was chosen to validate the sinusoidal model and a good fit was revealed between the derived total daytime net radiation and the measured data. Comparing with measured average daytime net radiation, the derived values are overestimated because of the overestimation in the retrieval of instantaneous net radiation. The statistics showed that the MAE of the retrieved results is $34.13\ W \cdot m^{-2}$ and the $RMSE$ is $36.12\ W \cdot m^{-2}$.

During the atmospheric correction of HJ satellite data, for convenience as well as the consideration that the aerosol retrieved from satellite data cannot be validated, the MODIS aerosol product (MOD04) was used to determine the aerosol optical depth. Many studies have been done on the aerosol retrieval from

HJ satellite data and such retrieval has been made possible, and the HJ satellite data can be used for atmospheric correction, thus eliminating the dependency on MODIS data. Meanwhile, the albedo conversion from narrow HJ satellite waveband to wide waveband was based on the radiative simulation of 6S model instead of generalized equations. A generalized equation can actually be constructed based on the algorithm of Liang [26]. In addition, limited by the availability of ground measurements, data of only three ground stations were used for retrieval modeling and accuracy evaluation. This may be improved by including more data.

Acknowledgements

This work was supported by National Natural Science Foundation of China, No. 41061024

References

1. Ye J, Liu H Z, Li W B, C.C. (2010) Estimation of the Net Radiation over Arid and Semiarid Areas Only Using MODIS Data for Clear Sky Days. Acta Scientiarum Naturalium Universitatis Pekinensis, 46(6), p.p.942-950.
2. Li Z, Tang R, Wan Z, C.C. (2009) A Review of Current Methodologies for Regional Evapotranspiration Estimation from Remotely Sensed Data. Sensors, 9(5), p.p.3801-3853.
3. Pinker R T, Tarpley J D, Laszlo I, C.C. (2003) Surface radiation budgets in support of the GEWEX Continental-Scale International Project (GCIP) and the GEWEX Americas Prediction Project (GAPP), including the North American Land Data Assimilation System (NLDAS) project. Journal of Geophysical Research: Atmospheres, 108(D22), p.p.8844.
4. Zhang Y, Rossow W B, Lacis A A, C.C. (2004) Calculation of radiative fluxes from the surface to top of atmosphere based on ISCCP and other global data sets: Refinements of the radiative transfer model and the input data. Journal of Geophysical Research: Atmospheres, 109(D19), p.p.D19105.
5. Wielicki B A, Div. A S, Center N L R, C.C. (1998) Clouds and the Earths Radiant Energy System (CERES): algorithm overview. IEEE Transactions on Geoscience and Remote Sensing, 36(4), p.p.1127-1141.
6. Samani Z, Tran V, Bleiwess M, C.C. (2013) Estimating Daily and 24-Hour Net Radiation for All Sky Conditions through Remote Sensing and Climatic Data. Journal of Irrigation and Drainage Engineering, 139(3), p.p.208-213.
7. Yu S S, Xin X Z, Liu Q H. (2013) Estimation of Clear-Sky Downward Atmospheric Longwave Radiation using HJ-1B Thermal Infrared Data. Scientia Sinica (Terrae), 43(2), p.p.256-270.
8. Ma Y, Zhong L, Wanga Y, C.C. (2012) Using NOAA/AVHRR data to determine regional net radiation and soil heat fluxes over the heterogeneous landscape of the Tibetan Plateau. International Journal of Remote Sensing, 33(15), p.p.4784-4795.
9. Dos Santos C, Do Nascimento R, Rao T, C.C. (2011) Net radiation estimation under pasture and forest in Rondônia, Brazil, with TM Landsat 5 images. Atmósfera, 24(4), p.p.435-446.
10. Bisht G, Bras R L. (2011) Estimation of Net Radiation From the Moderate Resolution Imaging Spectroradiometer Over the Continental United States. IEEE Transactions on Geoscience and Remote Sensing, 49(6), p.p.2448-2462.
11. Zhang H, Jiao Z T, Li X W, C.C. (2013) A Priori Knowledge Application in the Retrieval of Surface Albedo using HJ-1 CCD Data. Journal of Remote Sensing, 17(2), p.p.286-307.
12. Sobrino J A, Jiménez-Muñoz J C, Paolini L. (2004) Land surface temperature retrieval from LANDSAT TM 5. Remote Sensing of Environment, 90(4), p.p.434-440.
13. Zhou J, Li J, Zhao X, C.C. (2011) A Modified Single-Channel Algoritham for Land Surface Temprature Retrieval from HJ-1B Satellite Data. Journal of Infrared and Millimeter Waves, 30(1), p.p.61-67.
14. Xu J B, Zhao K, Zhao Z Z, C.C. (2013) Estimation of Near-Surface Air Temperature from HJ-1B Satellite Data in Northwest China. Transactions of the Chinese Society of Agricultural Engineering, 29, p.p.145-153.
15. Idso S B, Jackson R D. (1969) Thermal radiation from the atmosphere. Journal of Geophysical Research, 74(23), p.p.5397-5403.
16. Bastiaanssen W G M, Menenti M, Feddes R A, C.C. (1998) A remote sensing surface energy balance algorithm for land (SEBAL). 1. Formulation. Journal of Hydrology, 212–213(0), p.p.198-212.
17. Li X, Cheng G D, Liu S M, C.C. (2013) Heihe Watershed Allied Telemetry Experimental Research (HiWATER): Scientific objectives and experimental design. Bulletin of American Meteorological Society, 94(8), p.p.1145-1160.
18. Li X H, Huang X Q, Chi T H, C.C. (1993) Computation of Solar Elevations and Azimuths at Pixels of Satellite Image. Acta Geodaetica et

Cartographica Sinica, 22(2), p.p.149-154.
19. Kimes D S, Sellers P J. (1985) Inferring hemispherical reflectance of the earth's surface for global energy budgets from remotely sensed nadir or directional radiance values. Remote Sensing of Environment, 18(3), p.p.205-223.
20. Shuai Y, Masek J G, Gao F, C.C. (2011) An algorithm for the retrieval of 30-m snow-free albedo from Landsat surface reflectance and MODIS BRDF. Remote Sensing of Environment, 115(9), p.p.2204-2216.
21. Chulam Abduwasit, Qin Q M. (2007) Calculation of ETM+ Broadband Albedos by Radiative Simulations. Acta Scientiarum Naturalium Universitatis Pekinensis, p.p.474-483.
22. Nieto H, Sandholt I, Aguado I, C.C. (2011) Air temperature estimation with MSG-SEVIRI data: Calibration and validation of the TVX algorithm for the Iberian Peninsula. Remote Sensing of Environment, 115(1), p.p.107-116.
23. Wloczyk C, Borg E, Richter R, C.C. (2011) Estimation of instantaneous air temperature above vegetation and soil surfaces from Landsat 7 ETM+ data in northern Germany. International Journal of Remote Sensing., 32(24), p.p.9119-9136.
24. Ryu Y, Kang S, Moon S, C.C. (2008) Evaluation of land surface radiation balance derived from moderate resolution imaging spectroradiometer (MODIS) over complex terrain and heterogeneous landscape on clear sky days. Agricultural and Forest Meteorology, 148(10), p.p.1538-1552.
25. Sinnott R W. (1994) Sunrise and sunset: A challenge. Sky & Telescope, 88(2), p.p.84.
26. Liang S. (2001) Narrowband to broadband conversions of land surface albedo I: Algorithms. Remote Sensing of Environment, 76(2), p.p.213-238.

Convergence and Calculation Speed of Genetic Algorithm in Structural Engineering Optimization

Yunhua Zhu, Xiao Cai

College of Business Administration,
Huaqiao University, Quanzhou 362021,
Fujian, China

Abstract
In view of the existing genetic algorithm in structural engineering optimization has poor convergence, computational speed is slow, a optimization scheme of genetic algorithm is proposed in this paper based on the crossover operator and fitness function. The first use of the hybrid mechanism of the single point crossover operator of genetic algorithm is improved, in order to improve the searching space, and then the small to adapt to the optimization of the habitat mechanism of sharing function convergence. The simulation results show that, the crossover operator and fitness function based genetic algorithm optimization in structural engineering optimization has better, faster and better stability.